

# Predicting Catalytic Activity for CH<sub>4</sub> Combustion on Pd-exchanged Zeolite Catalysts Using Automated Reaction Route Mapping

Shiho Sakuma<sup>1</sup>, Shunsaku Yasumura<sup>1,\*</sup>, Kenichiro Saita<sup>2</sup>, Tetsuya Taketsugu<sup>2,3</sup>, Masaru Ogura<sup>1,\*</sup>

<sup>1</sup>Institute of Industrial Science, The University of Tokyo, Komaba 4-6-1, Meguro, Tokyo, Japan 153-8505

<sup>2</sup>Department of Chemistry, Faculty of Science, Hokkaido University, N10W8, Kita-ku Sapporo, Japan 060-0810

<sup>3</sup>Institute for Chemical Reaction Design and Discovery, Hokkaido University, N21W10, Kita-ku Sapporo, Japan 001-0020

## ABSTRACT

While computational predictions of catalytic activity are highly desired, conventional methods have difficulty capturing the complexity of reactions on solid catalyst surfaces. To address this issue, we employed a novel approach combining neural network potentials (NNPs) with automated reaction route mapping to explore reaction mechanisms of CH<sub>4</sub> combustion on Pd-exchanged zeolites (Pd-CHA, Pd-beta, and Pd-MOR). The predicted reaction map of CH<sub>4</sub> combustion over Pd<sup>2+</sup> site revealed partially oxidized species such as CH<sub>2</sub>O, HCOOH, and bicarbonate as the potential intermediates toward CO<sub>2</sub> + 2H<sub>2</sub>O. Activation energies ( $E_a$ ) of the rate-determining step (RDS) were evaluated, revealing the order of  $E_a$  as Pd-MOR < Pd-beta < Pd-CHA. A kinetic analysis using rate constant matrix contraction (RCMC) method estimated the catalytic activities of these catalysts. No reaction intermediates with significant lifetimes were observed on Pd-beta and Pd-MOR, whereas stable bicarbonate intermediates were present on Pd-CHA, decreasing the formation rate of CO<sub>2</sub> + 2H<sub>2</sub>O. Kinetic analysis further predicted the pseudo CO<sub>2</sub> formation rate with activity order Pd-MOR > Pd-beta > Pd-CHA, aligning with experimental results. These findings demonstrate the potential of the automated reaction route mapping with NNP for predicting the catalytic activity of solid catalysts, enabling their efficient pre-screening and rational design.

## 1. Introduction

Methane ( $\text{CH}_4$ ), the main component of natural gas, is widely used as a clean fuel in applications such as city gas, natural gas vehicles, and thermal power plants. However,  $\text{CH}_4$  is also a potent greenhouse gas and the second-largest contributor to global warming after carbon dioxide ( $\text{CO}_2$ ).<sup>1</sup> Because of its global warming potential, which is 22 times greater than that of  $\text{CO}_2$ , the reduction of  $\text{CH}_4$  emissions is required.<sup>2–4</sup>  $\text{CH}_4$  slip has been recognized as one of the major sources of  $\text{CH}_4$  emissions caused by the incomplete combustion of  $\text{CH}_4$  in fuels (unburned  $\text{CH}_4$ ). To address this issue, the development of efficient catalytic systems for the complete combustion of unburned  $\text{CH}_4$  is highly demanded.<sup>5,6</sup> Extensive research has been conducted on various types of catalysts, such as platinum group metals<sup>7–10</sup> to earth-abundant metal oxides.<sup>11–13</sup> Among reported catalysts, Pd-loaded  $\text{Al}_2\text{O}_3$  catalysts have shown exceptional catalytic activity, although this catalyst suffered from poisoning by water vapor and  $\text{SO}_2$  present in the exhaust gas, leading to rapid and irreversible deactivation.<sup>5,14,15</sup> In contrast, zeolite has been recognized as the catalyst support exhibiting superior durability compared to  $\text{Al}_2\text{O}_3$ .<sup>9,10,16</sup> Consequently, the development of highly active zeolite-based catalysts for  $\text{CH}_4$  combustion is strongly desired.

Zeolites exhibit diverse framework structures, and previous studies have demonstrated that the catalytic activity of Pd-loaded zeolites significantly depends on the framework type.<sup>16–20</sup> Since the changes in activity can be attributed to several factors, including acidity, pore size, and the states of the introduced metal cations, zeolite catalysts are often developed through extensive trial-and-error catalytic tests. The recent advancements in computational chemistry have drawn attention to predicting catalytic performance based on transition state (TS) calculations that evaluate the activation energy ( $E_a$ ) of each elemental reaction. Although TS calculation is a promising approach for screening catalytic activity, estimating the intricate elementary steps occurring on the rough solid catalyst surface is essential to evaluate the  $E_a$ . Thus, the computational prediction of catalytic activity remains a formidable task, particularly in heterogeneous catalysis. To overcome these challenges, advanced

techniques for comprehensive reaction path analysis are desired. One promising method is automated reaction route mapping technique to explore the whole reaction route of catalytic reactions. Maeda and co-workers have developed an artificial force induced reaction (AFIR) method that induces reactions by applying artificial attractive or repulsive forces between atoms (Figure 1a).<sup>21–23</sup> Applying the artificial force, which is proportional to the interatomic distance, to the potential energy function, the product of the reaction can be discovered by minimizing the AFIR function (Figure 1b). The AFIR function curve also stores the potential energy curve without any artificial forces, which is called the AFIR path. By optimizing the AFIR path and the subsequent transition state (TS) optimization and intrinsic reaction coordinate (IRC) calculations, new equilibrium (EQ) and TS structures can be obtained. This procedure is repeatedly conducted to map the reaction route without initial estimation of the products and possible reaction mechanisms.<sup>24</sup> Energy calculations for this reaction mapping are frequently performed using DFT calculations.<sup>24,25</sup> However, the computational cost is extensive, as more than one million energy calculations are required for the reaction mapping of solid catalysts. This requirement significantly hinders the computational screening of solid catalysts due to the prohibitive costs associated with these calculations.

Neural network potentials (NNPs) have recently attracted considerable attention owing to the remarkable capabilities of neural networks combined with extensive datasets. The Preferred Potential (PFP) is known as a “universal” NNP specifically designed to accommodate any mixture of elements.<sup>26</sup> PFP is trained by results generated from the Vienna ab initio Simulation Package (VASP) software, a widely recognized tool within the community of heterogeneous catalysis.<sup>27–29</sup> While the energy calculated by PFP does not entirely align with those obtained from VASP, they provide approximate results sufficient for a qualitative discussion of the reaction path.<sup>30</sup>

In this study, we applied an approach combining the PFP and AFIR (NNP-AFIR) methods to explore the entire reaction path for catalytic CH<sub>4</sub> combustion over Pd-CHA, Pd-beta, and Pd-MOR. First, the reaction network from reactants (CH<sub>4</sub> + 2O<sub>2</sub>) over isolated Pd<sup>2+</sup> cation was explored using NNP-AFIR

to map the reaction routes for each zeolite catalyst (Figure 2a). The rate constant matrix contraction (RCMC) method, an efficient kinetic analysis developed specifically to analyze the complex reaction networks generated by the AFIR method, was applied to visualize the changes in the population of chemical species over time.<sup>23</sup> This approach takes into account the influence of side reactions and reverse reactions (Figure 2b). Then, the rate of products was compared among the catalysts and to the experimental result of the catalytic test (Figure 2c).

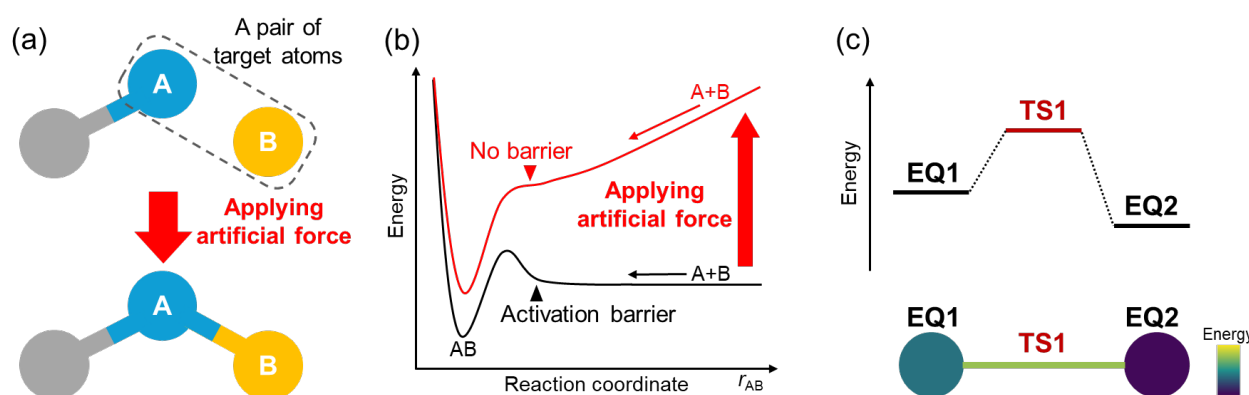


Figure 1 (a) Schematic representation of an artificial force induced reaction. (b) The diatomic potential curve for A and B forming AB (black curve) and the AFIR function curve (red curve), where  $r_{AB}$  is the interatomic distance. (c) Energy profile of an elementary process and corresponding graph representation. The nodes and edges represent EQs and TSs that connect them. Their colors represent the relative energy.

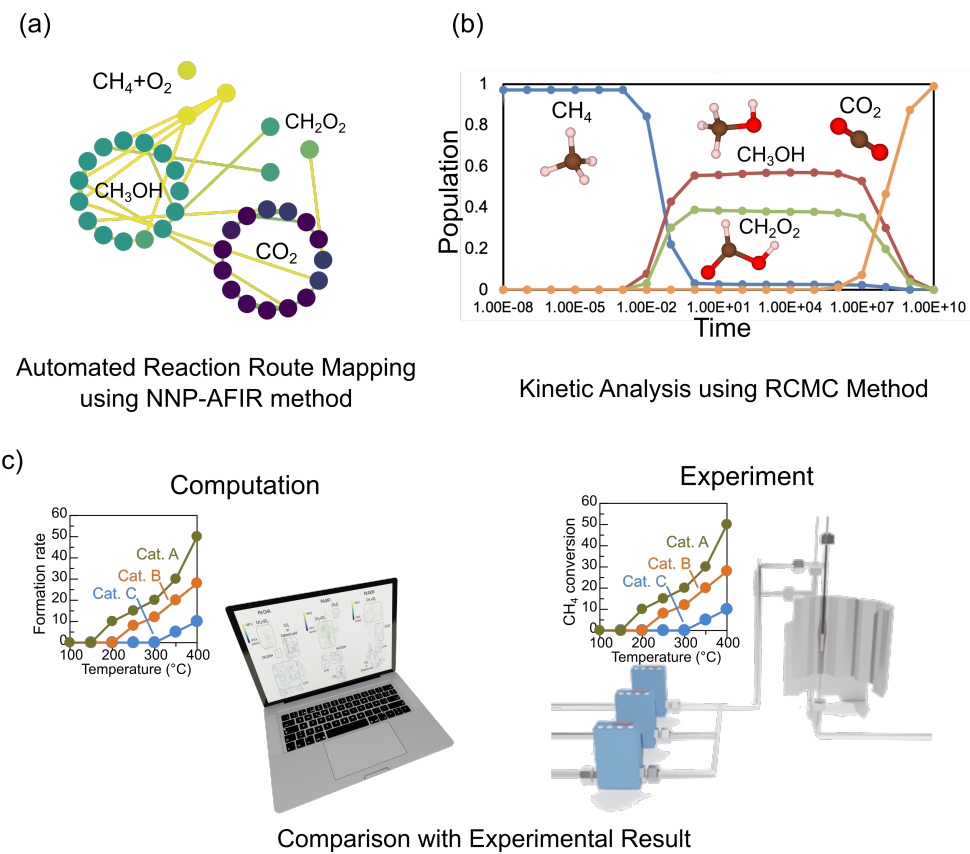


Figure 2 The computational prediction of catalytic activity using (a) NNP-AFIR and (b) RCMC methods, and (c) the following comparison of computational result and experimental catalytic test.

## 2. Results

### 2.1 Reaction route mapping using neural network potential

The reaction routes of  $\text{CH}_4 + 2\text{O}_2$  reaction over Pd-exchanged zeolites were mapped using the NNP-AFIR method. Among the types of AFIR methods, Single-component AFIR (SC-AFIR) was applied in this study. The upper part of Figure 3 shows the periodic structure model of (a) CHA, (b) beta, and (c) MOR zeolites obtained from IZA database.<sup>31</sup> Among the distinguished T sites for beta zeolites, two T6 sites were substituted with Al to construct the 2Al sites, which were identified as the most favorable positioning.<sup>32</sup> In the case of MOR zeolite, two T1 sites were replaced.<sup>33</sup> CHA zeolite has only one T site due to its highly symmetric framework. The third nearest neighbor in the six-membered ring (6MR3NN) site was adopted in this study.<sup>34</sup> The  $\text{Pd}^{2+}$  cation was placed at the 2Al sites of the CHA, beta, and MOR zeolite frameworks. Additionally, a single  $\text{CH}_4$  and two  $\text{O}_2$  molecules were introduced as reactants.

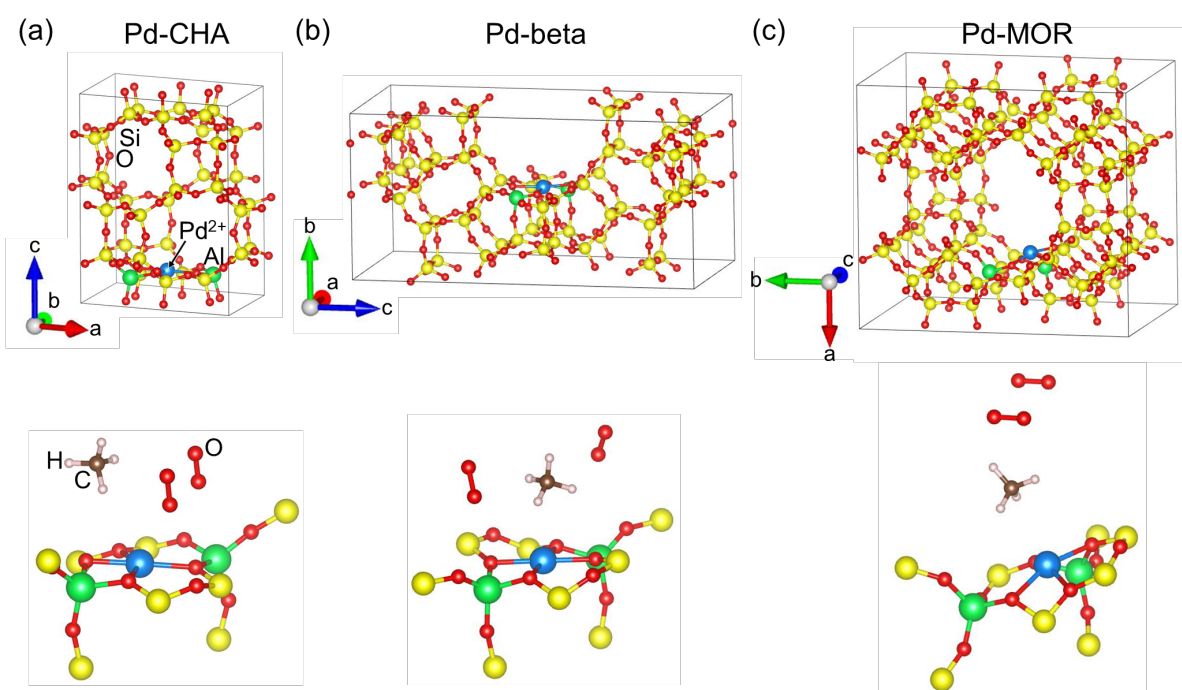


Figure 3 Unit cell models (upper) and starting structure for the reaction route mapping (lower) of (a) Pd-CHA, (b) Pd-beta, (c) Pd-MOR used in this study.

The resulting reaction routes for the  $\text{CH}_4 + 2\text{O}_2$  reaction over Pd-CHA, Pd-beta, and Pd-MOR catalysts are displayed in Figure 4. The nodes correspond to EQs, and the edges represent TSs or approximate transition states called path-tops (PTs; Figure 1c). Their colors indicate relative energy levels, as shown in the color bar on the right. By grouping similar structures of EQs, we identified key species such as the initial reactant  $\text{CH}_4$ , the intermediate formaldehyde ( $\text{CH}_2\text{O}$ ), Formic acid ( $\text{HCOOH}$ ),  $\text{CO}$ , and the final product  $\text{CO}_2$ . The analysis indicates that EQs with similar structures exhibit comparable energy, with multiple routes connecting these groups. This interconnected network suggests that  $\text{CH}_4$  combustion proceeds through complex reaction routes toward  $\text{CO}_2$  as the most stable species.

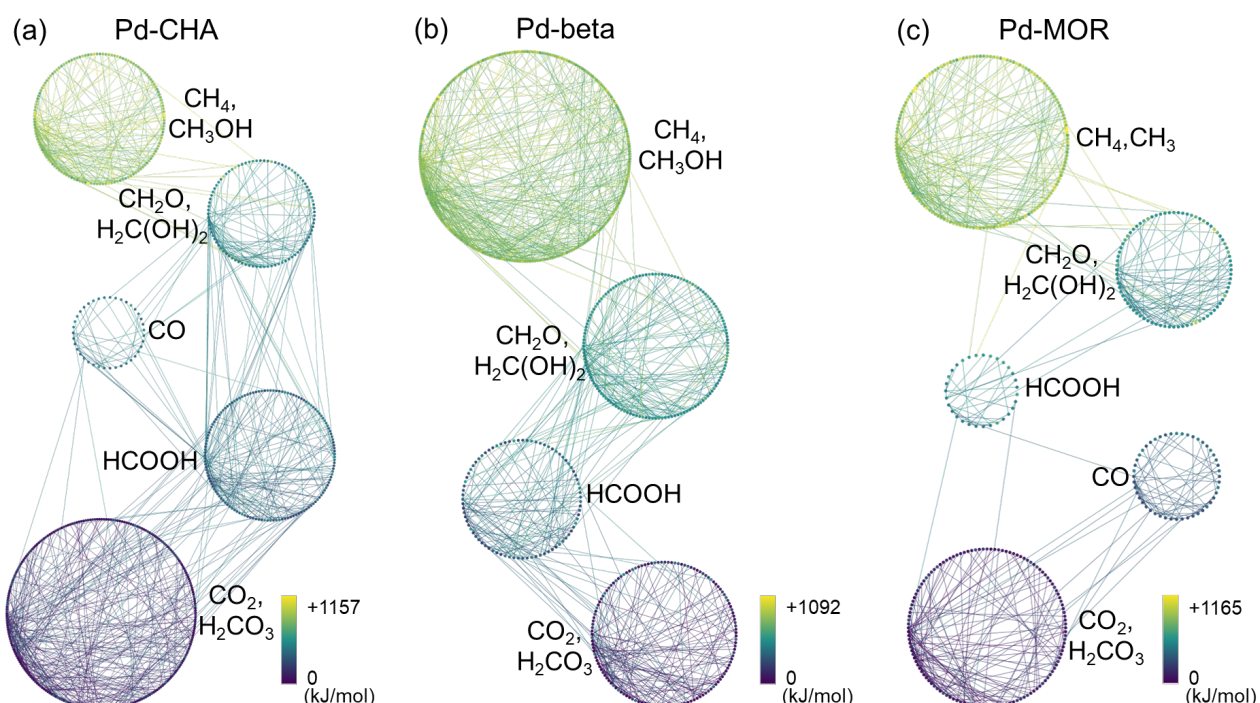


Figure 4 Reaction route maps for  $\text{CH}_4$  combustion over (a) Pd-CHA, (b) Pd-beta, and (c) Pd-MOR catalysts, highlighting key intermediates and interconnected routes facilitating the reaction progression. Nodes and edges describe obtained structures and paths linking them (TSs and PTs, determined by GRRM software), respectively. Their colors represent the relative energy (the color bar is shown on the bottom right).

Figure 5 shows the energy profile along the main reaction route of methane combustion, extracted from the reaction route map. The reaction route begins with the EQ structure corresponding to  $\text{CH}_4 + 2\text{O}_2$  and proceeds toward the EQ structure corresponding to  $\text{CO}_2 + 2\text{H}_2\text{O}$ . For Pd-CHA,  $\text{CH}_4 + 2\text{O}_2$  reacts via a high  $E_a$  to form  $\text{CH}_3\text{OOH} + \text{O}_2$  (EQ16;  $E_a = 153 \text{ kJ/mol}$ ), followed by another high activation barrier leading to the formation of  $\text{CH}_2\text{O} + \text{H}_2\text{O} + \text{O}_2$  (EQ107;  $E_a = 160 \text{ kJ/mol}$ ). Subsequent structural changes occur via intermediates such as  $\text{HCOOH}$ , bicarbonate, and formate, yielding  $\text{CO}_2 + 2\text{H}_2\text{O}$  (EQ276). For Pd-beta,  $\text{CH}_4 + 2\text{O}_2$  initially reacts through a high  $E_a$  to generate methanol ( $\text{CH}_3\text{OH}$ ) +  $\text{O}$  +  $\text{O}_2$  (EQ21;  $E_a = 156 \text{ kJ/mol}$ ), and the subsequent oxidation to  $\text{CO}_2 + 2\text{H}_2\text{O}$  (EQ163) proceeds via a different path. In contrast, Pd-MOR facilitates the generation of  $\text{CH}_3\text{OOH} + \text{O}_2$  (EQ206) through a relatively lower  $E_a$  (80 kJ/mol and 64 kJ/mol), and the reaction proceeds toward  $\text{CO}_2 + 2\text{H}_2\text{O}$  (EQ540) without high  $E_a$ . In the previous study, *in situ* DRIFTS for Pd-exchanged zeolite revealed that  $\text{CH}_4$  was oxidized into formate and carbonate species in a step-by-step manner,<sup>35</sup> which agrees with our computed reaction pathways. The values of  $E_a$  for the rate-determining step (RDS) of Pd-CHA, Pd-beta, and Pd-MOR were 160, 156, and 150 kJ/mol, respectively (comparisons of  $E_a$  for RDS obtained from VASP can be found in Table S1).

Bader charge analysis was performed to further investigate the factors influencing differences in catalyst activation barriers. The results revealed that lower Pd cationicity leads to a decrease in the activation energy ( $E_a$ ) of the rate-determining step (RDS) in methane combustion (Figure S1).

The obtained energy profiles imply that not only  $E_a$  for RDS but also those for other elementary steps are relatively high. In light of the observed complexity and the various transition states, it is obvious that focusing solely on the comparison of  $E_a$  for RDS does not reflect actual catalytic activities of each Pd-exchanged catalyst.

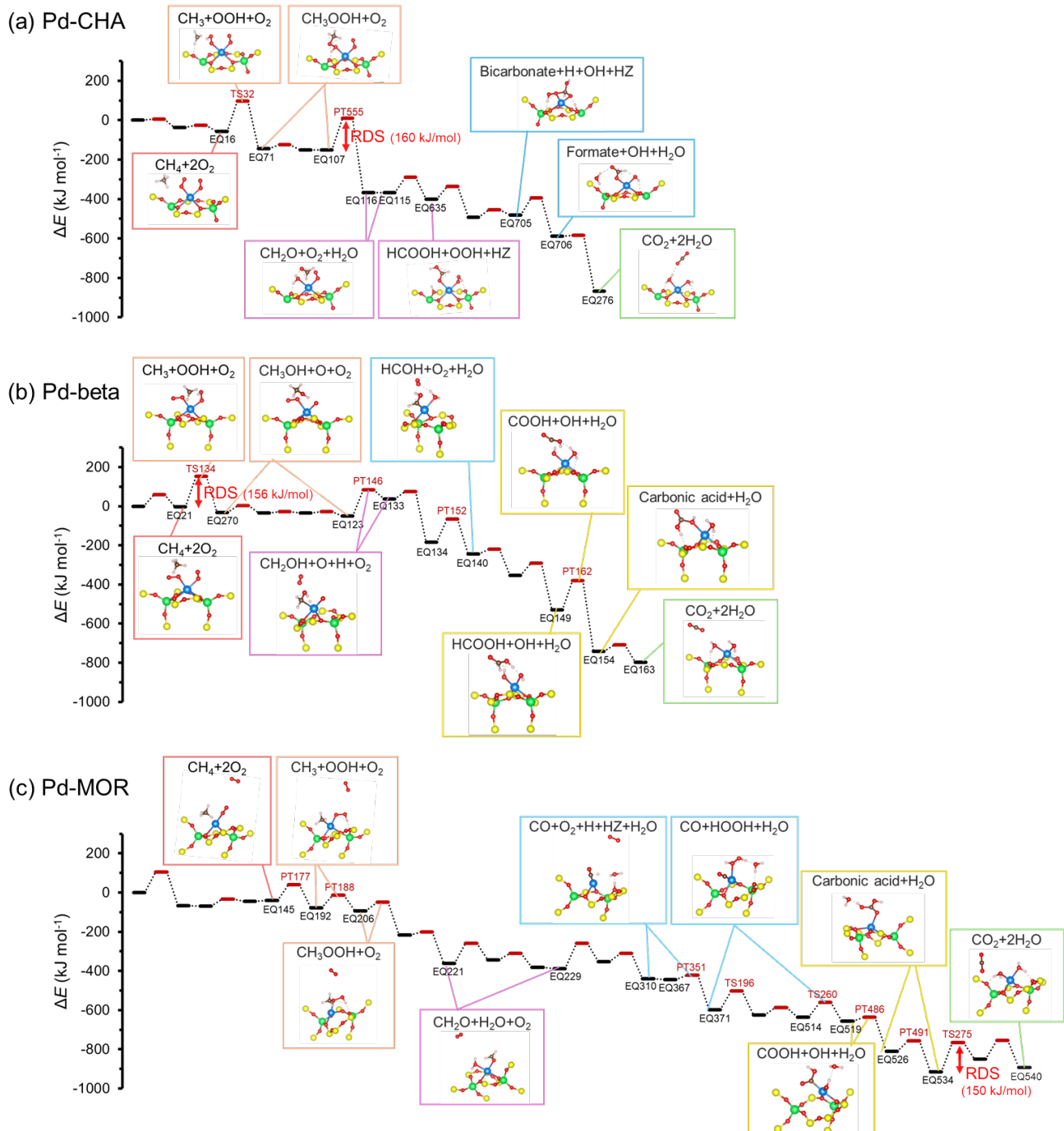


Figure 5 Energy profiles along with main reaction route for  $\text{CH}_4$  combustion over (a) Pd-CHA, (b) Pd-beta, and (c) Pd-MOR catalysts.

## 2.2 Comprehensive kinetic analysis and prediction of catalytic activity

Since catalytic reactions involve tremendous reaction routes comprising both fast and slow elementary reactions, the overall activity can be influenced not only by RDS but also by the entire reaction profile. To comprehensively evaluate catalytic activity, kinetic analysis was conducted using the RCMC method developed by Sumiya et al.<sup>36</sup> The RCMC method systematically reduces the rate constant matrix to group molecular structures into “superstates,” which appear and disappear within a specified reaction time parameter ( $t_{MAX}$ ), thereby enabling efficient kinetic analysis for the huge reaction maps (809 of EQ and 1196 of TS and PT, in the case of Pd-CHA). By applying RCMC across different reaction periods, structural changes over time can be effectively visualized as the population of each chemical species.<sup>22,37</sup>

Figure 6 shows the variation in the population of surface-adsorbed species on the catalysts over a simulation period of  $10^{-10}$  to  $10^{10}$  seconds at 500°C. This time window ensures the inclusion of reaction rates of diverse solid catalysts.<sup>38</sup> As the main product, the CO<sub>2</sub> and two H<sub>2</sub>O molecules are expected for all catalysts. Only in the case of Pd-CHA, bicarbonate intermediate appeared with a long lifetime. The intermediates CH<sub>3</sub>OO and CH<sub>2</sub>O on Pd-beta and Pd-MOR, respectively, were observed, although their populations did not exhibit a significant increase, indicating that these intermediates are short-lived and are rapidly converted into CO<sub>2</sub> and 2H<sub>2</sub>O.

The catalytic activity was evaluated using  $t_{0.5}$ , defined as the time at which the population of the target species reaches 0.5. This metric serves as a key indicator of reaction rate, enabling a comparison of the kinetic behavior under different temperatures among different catalysts (Figure S2). A shorter  $t_{0.5}$  indicates faster formation of CO<sub>2</sub> + 2H<sub>2</sub>O, reflecting higher catalytic activity. Figure 7a compares  $t_{0.5}$  across zeolites at different temperatures. The results showed the catalytic activity order of Pd-MOR > Pd-beta > Pd-CHA.

We conducted catalytic tests to experimentally validate the catalytic activity expected by the kinetic analysis. Figure 7b shows the catalytic activity results. The observed activity trend (Pd-MOR > Pd-

$\beta$  > Pd-CHA) is consistent with the predictions from the calculations, demonstrating that the computational approach employed in this study qualitatively reproduced the experimental catalytic activity, achieving virtual screening of Pd-exchanged zeolite catalysis without any experimental parameters.

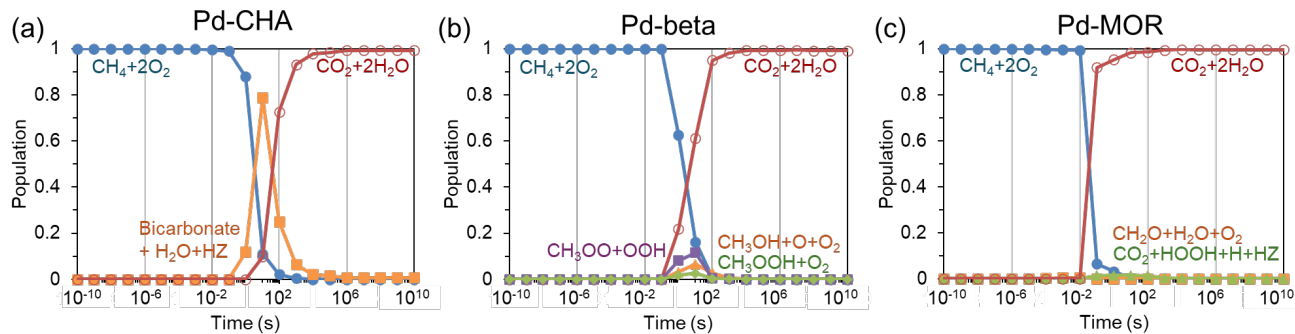


Figure 6 Time evolution of the population of surface-adsorbed species on (a) Pd-CHA, (b) Pd-beta, and (c) Pd-MOR during the transformation of  $\text{CH}_4 + 2\text{O}_2$  to  $\text{CO}_2 + 2\text{H}_2\text{O}$  at  $500^\circ\text{C}$ , obtained through RCMC simulations over a range of  $10^{-10}$  to  $10^{10}$  seconds.

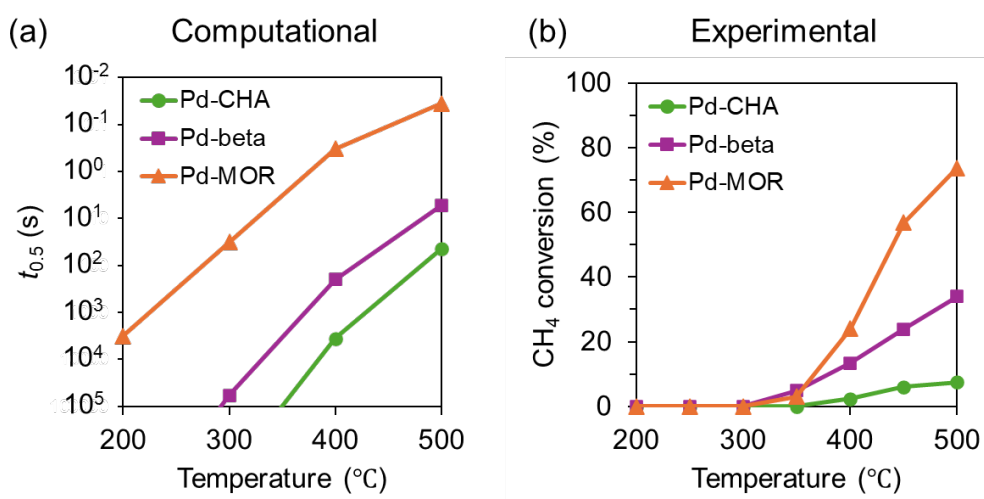


Figure 7 (a) Computational prediction of catalytic activity based on kinetic simulations using the RCMC method. (b) Experimental catalytic test measured in a fixed-bed flow reactor under reaction conditions of 0.1%  $\text{CH}_4 + 10\%$   $\text{O}_2$  (total flow rate: 100 ml/min,  $\text{N}_2$  balance).

### 3. Discussion

In this study, a combined method of NNP and AFIR was utilized to predict computationally the CH<sub>4</sub> combustion activity of Pd-exchanged zeolite catalysts with different topologies (Pd-CHA, Pd-beta, and Pd-MOR). The entire reaction pathway from CH<sub>4</sub> + 2O<sub>2</sub> to CO<sub>2</sub> was systematically mapped using this approach. Subsequent analysis of the reaction maps revealed interconnected pathways featuring key intermediates such as CH<sub>3</sub>OH, CH<sub>3</sub>OOH, CH<sub>2</sub>O, HCOOH, formate, and bicarbonate, which were eventually oxidized to CO<sub>2</sub> and H<sub>2</sub>O. Notably, RDS exhibited  $E_a$  of 160, 156, and 150 kJ/mol for Pd-CHA, Pd-beta, and Pd-MOR, respectively. However, other steps also showed relatively high  $E_a$ , indicating that thermodynamics alone cannot fully capture the reaction's complexity. A comprehensive kinetic analysis was then conducted based on the identified reaction routes, considering the effects of side reactions and reverse reactions. In this analysis, the RCMC method was applied to monitor the time evolution of intermediates population. The plotted time evolution of the population of intermediates reveals that a long lifetime species (bicarbonate) on Pd-CHA, hindering reaction progress, while their rapid consumption and CO<sub>2</sub> formation were exhibited on Pd-beta and Pd-MOR. The rate of CO<sub>2</sub> formation was estimated, and the order of catalytic activity was determined as Pd-MOR > Pd-beta > Pd-CHA. To validate these findings, the corresponding Pd-exchanged zeolite catalysts were prepared, and their activities were evaluated experimentally. The results aligned well with computational predictions, confirming that the combined NNP-AFIR approach accurately captures the overall reaction profile and enables efficient catalyst screening. The NNP-AFIR method is expected to significantly decrease the number of experiments needed, thereby accelerating the development of solid catalysts.

## Methods

### Catalyst preparation

CHA-type zeolite (Tosoh, NH<sub>4</sub>-type, SiO<sub>2</sub>/Al<sub>2</sub>O<sub>3</sub> = 24.7), beta-type zeolite (JRC-Z-B25, Na-type, SiO<sub>2</sub>/Al<sub>2</sub>O<sub>3</sub> = 25), and MOR-type zeolite (JRC-Z-HM20, H-type, SiO<sub>2</sub>/Al<sub>2</sub>O<sub>3</sub> = 20) were employed in this study. The beta and MOR type-zeolites were supplied by Catalysis Society of Japan. The NH<sub>4</sub>-type CHA zeolite was calcined to its H-type form before the impregnation. Na-type beta zeolite was first subjected to an ion-exchange into NH<sub>4</sub>-type one with NH<sub>4</sub>NO<sub>3</sub> and then calcined into H-type form. Pd was loaded on the zeolites via solid-state ion exchange.<sup>39</sup> To achieve a Pd loading of 0.5 wt%, 1 ml of Pd(NO<sub>3</sub>)<sub>2</sub>·2H<sub>2</sub>O (5 mg Pd /ml, Wako) was added to 1 g of zeolite. Subsequently, 50 ml of water was added, and the mixture was stirred in an oil bath at 80°C. After evaporating the water, the impregnated zeolite was calcined at 500°C for 1 h in the air. The resulting samples were then placed in a flow reactor and subjected to a reduction treatment with 4% H<sub>2</sub>/He at 600°C for 30 min. This was followed by exposure to a flow of 4% NO at 600°C for 30 min and 100% O<sub>2</sub> at 700°C for 30 min to obtain ion-exchanged zeolites.

### CH<sub>4</sub> combustion test

The CH<sub>4</sub> combustion test was carried out under a flow of 0.1% CH<sub>4</sub> +10% O<sub>2</sub> (N<sub>2</sub> balance, total flow:100 ml/min) as a typical condition. Catalyst powders were put in the fixed-bed flow reactor using quartz wool. VA-3000 Gas Analyzer was connected to a VA-3000 Rack-Mounted Sample Gas Conditioning System (Horiba, Ltd) to monitor the outlet concentrations of CH<sub>4</sub> and CO<sub>2</sub>.

## Computational details

The structural optimization was carried out using PFP (version 5.0.0, CRYSTAL\_U0\_PLUS\_D3 mode: crystal systems, with D3 dispersion correction) In this study, the Hubbard U correction was not applied because Pd is a 4d electron system with limited orbital delocalization.

The structures of the three zeolites were obtained from the International Zeolite Association (IZA) database, and the lattice constants were fixed at their initial values during the calculations: CHA ( $a = 13.6750 \text{ \AA}$ ,  $b = 13.6750 \text{ \AA}$ ,  $c = 14.7670 \text{ \AA}$ ,  $\alpha = \beta = 90.000^\circ$ ,  $\gamma = 120.000^\circ$ ), beta ( $a = 12.6614 \text{ \AA}$ ,  $b = 12.6614 \text{ \AA}$ ,  $c = 26.4061 \text{ \AA}$ ,  $\alpha = \beta = \gamma = 90.0^\circ$ ), and MOR ( $a = 18.2560 \text{ \AA}$ ,  $b = 20.5340 \text{ \AA}$ ,  $c = 15.0840 \text{ \AA}$ ,  $\alpha = \beta = \gamma = 90.0^\circ$ ). The SC-AFIR method, as implemented in the GRRM20 program<sup>40</sup>, was applied for reaction route mapping with a model collision energy parameter of  $\gamma = 1200 \text{ kJ/mol}$ . Only a positive force was applied in the AFIR calculations. The collision energy was applied to the H, O, and C atoms in the CH<sub>4</sub> and O<sub>2</sub> molecules, and the Pd cation positioned at the 2Al site, as targets of SC-AFIR. Additionally, Si atoms adjacent to Al and the O atoms bonded to these adjacent Si atoms were treated as active atoms (Figure 3, lower figure). All other atoms in the zeolite framework were constrained to their crystallographic positions as frozen atoms. The resulting structures are visualized by VESTA.<sup>41</sup>

## Artificial force induced reaction (AFIR)

We utilized the single-component algorithm of artificial force induced reaction (SC-AFIR) method, as implemented in the GRRM20 program, to perform reaction route mapping. This method enables the unbiased exploration of reaction pathways by simply providing an initial structure for investigation without human intervention. The core principle involves applying an artificial force to a pair of atoms within the system, governed by the following equation:

$$F^{AFIR}(Q) = E(Q) + \rho\alpha \frac{\sum_{i \in A} \sum_{j \in B} \omega_{ij} r_{ij}}{\sum_{i \in A} \sum_{j \in B} \omega_{ij}} \quad (1)$$

Here,  $E(Q)$  represents the potential energy as a function of the geometric parameter  $Q$ . In the second term, an artificial force is applied to the system, where the strength of this force is controlled by the

parameter  $\alpha$ , and  $\rho$  is set to either 1 (attractive) or -1 (repulsive). The term  $r_{ij}$  represents the interatomic distance between atoms  $i$  and  $j$  in fragments A and B, respectively. The weighting factor  $\omega_{ij}$  is defined as:

$$\omega_{ij} = \left[ \frac{R_i + R_j}{r_{ij}} \right]^6 \quad (2)$$

where  $R_i$  and  $R_j$  are the covalent radii of atoms  $i$  and  $j$ , respectively. For a more comprehensive explanation of the theoretical framework, refer to the developer's publication.<sup>40</sup>

## Kinetic analysis of reaction pathways

To conduct kinetic analysis of the obtained reaction routes, we used rate constant matrix contraction (RCMC) method, which is also implemented in the GRRM20 program. For a reaction network containing  $N$  equilibrium structures (EQs), an  $N \times N$  rate constant matrix is constructed. These rate constant matrices are obtained using conventional transition state theory (TST). When assuming a canonical ensemble, the rate constant based on TST is expressed as follows:

$$k_{X \rightarrow Y} = \Gamma \frac{k_B T}{h} \exp\left(-\frac{\Delta G_{TS} - \Delta G_X}{RT}\right) \quad (3)$$

where  $k_{X \rightarrow Y}$  is the rate constant for the reaction pathway from EQ<sub>X</sub> to EQ<sub>Y</sub>.  $k_B$ ,  $h$ ,  $R$ ,  $T$  and  $\Gamma$  represent the Boltzmann constant, Planck constant, gas constant, temperature, and transmission coefficient, respectively. The RCMC method simplifies the original  $N \times N$  rate constant matrix by reducing it to an  $n \times n$  matrix through an iterative contraction process applied  $M$  times, where  $N - n = M$ . This contraction is performed for all states with lifetimes shorter than a predefined reaction time  $t_{MAX}$ . The resulting  $n \times n$  rate constant matrix describes transitions between  $n$  superstates, where each superstate is a weighted combination of multiple EQs. In other words, EQs grouped into the same superstate can interconvert on a timescale shorter than  $t_{MAX}$ . By conducting RCMC with varying values of  $t_{MAX}$ , the time hierarchy of the reaction network and the time evolution of an initial population assigned to

arbitrary EQs can be explored. For a more detailed discussion of the theoretical framework, please refer to the original publication by the method's developers.<sup>36</sup>

## Competing interest statement

The authors declare no competing interests.

## Author contributions

S.S wore the draft and carried out reaction route mapping and catalytic test. S.Y, K.S, and T.T deeply discussed the applied computational approach and critically supported the utilization of the NNP-AFIR method. S.Y, K.S, and T.T critically revised the manuscript. S.Y and M.O designed and supervised the whole project.

## Statistics & Reproducibility

The experiments were not randomized.

## Data availability:

The source data, which support the result of this study, can be found in the manuscript and Supplementary information. Data are available from the corresponding author upon request.

## Code availability:

The Matlantis, GRRM, and VASP code package used in this work can be accessible after a user license is authorized (Matlantis: <https://matlantis.com>, GRRM: <https://global.hpc.co.jp/products/grrm23/>, VASP: <https://www.vasp.at>). VESTA can be freely accessible from the websites (VESTA: <https://jp-minerals.org/vesta/en/>)

## ACKNOWLEDGEMENTS

This research was funded by KAKENHI (23K19175) from the Japan Society for the Promotion of Science (JSPS). S.Y. gratefully acknowledges the support from Daiichi-Sankyo "Habataku" Support Program for the Next Generation of Researchers, Koyanagi-Foundation, and Kazuchika Okura Memorial Foundation. K.S and T.T are grateful for the grant from the Photo-Excitonix Project at Hokkaido University. Part of the results in this research were obtained using supercomputing resources at Cyberscience Center, Tohoku University.

## REFERENCES

1. World Meteorological Organization (WMO). WMO Greenhouse Gas Bulletin No. 20. *World Meteorological Organization* (2024).
2. Grant Allen. Rebalancing the global methane budget. *Nature* **538**, 46–48 (2016).
3. Schwietzke, S. *et al.* Upward revision of global fossil fuel methane emissions based on isotope database. *Nature* **538**, 88–91 (2016).
4. Montzka, S. A., Dlugokencky, E. J. & Butler, J. H. Non-CO<sub>2</sub> greenhouse gases and climate change. *Nature* **476**, 43–50 (2011).
5. He, L., Fan, Y., Bellette, J., Yue, J. & Luo, L. A review on catalytic methane combustion at low temperatures: Catalysts, mechanisms, reaction conditions and reactor designs. *Renewable and Sustainable Energy Reviews* **119**, 109589 (2020).
6. Chen, J., Arandiyan, H., Gao, X. & Li, J. Recent Advances in Catalysts for Methane Combustion. *Catalysis Surveys from Asia* **19**, 140–171 (2015).
7. Gélin, P. & Primet, M. Complete oxidation of methane at low temperature over noble metal based catalysts: a review. *Appl Catal B* **39**, 1–37 (2002).
8. Ciuparu, D., Lyubovsky, M. R., Altman, E., Pfefferle, L. D. & Datye, A. Catalytic combustion of methane over palladium-based catalysts. *Catal Rev Sci Eng* **44**, 593–649 (2002).
9. Petrov, A. W. *et al.* Stable complete methane oxidation over palladium based zeolite catalysts. *Nat Commun* **9**, 2545 (2018).
10. Jiang, D., Khivantsev, K. & Wang, Y. Low-Temperature Methane Oxidation for Efficient Emission Control in Natural Gas Vehicles: Pd and beyond. *ACS Catal* **10**, 14304–14314 (2020).
11. Arai, H., Yamada, T., Eguchi, K. & Seiyama, T. Catalytic Combustion of Methane Over Various Perovskite-type. *Appl Catal* **26**, 265–276 (1986).
12. Ferri, D. & Forni, L. Methane combustion on some perovskite-like mixed oxides. *Appl Catal B* **16**, 119–126 (1998).
13. Tao, F. F. *et al.* Understanding complete oxidation of methane on spinel oxides at a molecular level. *Nat Commun* **6**, 7798 (2015).
14. Yoshida, H., Nakajima, T., Yazawa, Y. & Hattori, T. Support effect on methane combustion over palladium catalysts. *Appl Catal B* **71**, 70–79 (2007).
15. Baldwin, T. R. & Burch, R. Catalytic combustion of methane over supported palladium catalysts II. Support and possible morphological effects. *Appl Catal* **66**, 359–381 (1990).
16. Chen, H. Y., Lu, J., Fedeyko, J. M. & Raj, A. Zeolite supported Pd catalysts for the complete oxidation of methane: A critical review. *Appl Catal A Gen* **633**, (2022).
17. Tan, X. & Hong, S. B. A highly active and stable palladium zeolite catalyst for wet methane combustion. *Appl Catal B* **361**, 124562 (2025).

18. Park, J. H. *et al.* Methane combustion over Pd catalysts loaded on medium and large pore zeolites. *Top Catal* **52**, 27–34 (2009).
19. Nomura, K. *et al.* Pd-Pt bimetallic catalyst supported on SAPO-5 for catalytic combustion of diluted methane in the presence of water vapor. *Catal Letters* **53**, 167–169 (1998).
20. Montes de Correa, C. & Luz Villa, A. H. Combustion of methane over palladium ZSM-5 and mordenite catalysts. *Appl Catal B* **10**, 313–323 (1996).
21. Maeda, S., Sugiyama, K., Sumiya, Y., Takagi, M. & Saita, K. Global reaction route mapping for surface adsorbed molecules: A case study for H<sub>2</sub>O on Cu(111) surface. *Chem Lett* **47**, 396–399 (2018).
22. Sugiyama, K., Saita, K. & Maeda, S. A reaction route network for methanol decomposition on a Pt(111) surface. *J Comput Chem* **42**, 2163–2169 (2021).
23. Sugiyama, K., Sumiya, Y., Takagi, M., Saita, K. & Maeda, S. Understanding CO oxidation on the Pt(111) surface based on a reaction route network. *Physical Chemistry Chemical Physics* **21**, 14366–14375 (2019).
24. Maeda, S., Taketsugu, T. & Morokuma, K. Exploring transition state structures for intramolecular pathways by the artificial force induced reaction method. *J Comput Chem* **35**, 166–173 (2014).
25. Nabata, H., Takagi, M., Saita, K. & Maeda, S. Computational searches for crystal structures of dioxides of group 14 elements (CO<sub>2</sub>, SiO<sub>2</sub>, GeO<sub>2</sub>) under ultrahigh pressure. *RSC Adv* **10**, 22156–22163 (2020).
26. Takamoto, S. *et al.* Towards universal neural network potential for material discovery applicable to arbitrary combination of 45 elements. *Nat Commun* **13**, 2991 (2022).
27. Li, G., Pidko, E. A., Van Santen, R. A., Li, C. & Hensen, E. J. M. Stability of extraframework iron-containing complexes in ZSM-5 zeolite. *Journal of Physical Chemistry C* **117**, 413–426 (2013).
28. Chen, B. W. J., Xu, L. & Mavrikakis, M. Computational Methods in Heterogeneous Catalysis. *Chem Rev* **121**, 1007–1048 (2021).
29. Latimer, A. A. *et al.* Understanding trends in C-H bond activation in heterogeneous catalysis. *Nat Mater* **16**, 225–229 (2017).
30. Staub, R., Gantzer, P., Harabuchi, Y., Maeda, S. & Varnek, A. Challenges for Kinetics Predictions via Neural Network Potentials: A Wilkinson’s Catalyst Case. *Molecules* **28**, 4477 (2023).
31. Ch. Baerlocher, Darren Brouwer, Bernd Marler & L.B. McCusker. Database of Zeolite Structures. <http://www.iza-structure.org/databases/>.
32. Vorontsov, A. V. & Smirniotis, P. G. DFT Study on the Stability and the Acid Strength of Brønsted Acid Sites in Zeolite β. *Journal of Physical Chemistry A* **126**, 7840–7851 (2022).
33. Grybos, R., Hafner, J., Benco, L. & Raybaud, P. Adsorption of NO on Pd-exchanged mordenite: Ab initio DFT modeling. *Journal of Physical Chemistry C* **112**, 12349–12362 (2008).

34. Yasumura, S. *et al.* Local structure and NO adsorption/desorption property of Pd<sup>2+</sup>cations at different paired Al sites in CHA zeolite. *Physical Chemistry Chemical Physics* **23**, 22273–22282 (2021).
35. Gao, M. *et al.* Methane combustion over palladium catalyst within the confined space of MFI zeolite. *Chinese Journal of Catalysis* **42**, 1689–1699 (2021).
36. Sumiya, Y. & Maeda, S. Rate constant matrix contraction method for systematic analysis of reaction path networks. *Chem Lett* **49**, 553–564 (2020).
37. Sumiya, Y., Nagahata, Y., Komatsuzaki, T., Taketsugu, T. & Maeda, S. Kinetic Analysis for the Multistep Profiles of Organic Reactions: Significance of the Conformational Entropy on the Rate Constants of the Claisen Rearrangement. *Journal of Physical Chemistry A* **119**, 11641–11649 (2015).
38. Medford, A. J. *et al.* From the Sabatier principle to a predictive theory of transition-metal heterogeneous catalysis. *J Catal* **328**, 36–42 (2015).
39. Yasumura, S. *et al.* Transformation of Bulk Pd to Pd Cations in Small-Pore CHA Zeolites Facilitated by NO. *JACS Au* **1**, 201–211 (2021).
40. Maeda, S., Harabuchi, Y., Takagi, M., Taketsugu, T. & Morokuma, K. Artificial Force Induced Reaction (AFIR) Method for Exploring Quantum Chemical Potential Energy Surfaces. *Chemical Record* **16**, 2232–2248 (2016).
41. Momma, K. & Izumi, F. VESTA 3 for three-dimensional visualization of crystal, volumetric and morphology data. *J Appl Crystallogr* **44**, 1272–1276 (2011).